J. Phycol. **48,** 635–646 (2012)
© 2012 Phycological Society of America
DOI: 10.1111/j.1529-8817.2012.01171.x

ELEVATED CARBON DIOXIDE DIFFERENTIALLY ALTERS THE PHOTOPHYSIOLOGY OF *THALASSIOSIRA PSEUDONANA* (BACILLARIOPHYCEAE) AND *EMILIANIA HUXLEYI* (HAPTOPHYTA)[1]

Avery McCarthy[2], *Susan P. Rogers, Stephen J. Duffy, and Douglas A. Campbell*[3]

Department of Chemistry & Biochemistry, Mount Allison University, Sackville, New Brunswick, E4L 1G7, Canada

Increasing anthropogenic carbon dioxide is causing changes to ocean chemistry, which will continue in a predictable manner. Dissolution of additional atmospheric carbon dioxide leads to increased concentrations of dissolved carbon dioxide and bicarbonate and decreased pH in ocean water. The concomitant effects on phytoplankton ecophysiology, leading potentially to changes in community structure, are now a focus of concern. Therefore, we grew the coccolithophore *Emiliania huxleyi* (Lohmann) W. W. Hay et H. Mohler and the diatom strains *Thalassiosira pseudonana* (Hust.) Hasle et Heimdal CCMP 1014 and *T. pseudonana* CCMP 1335 under low light in turbidostat photobioreactors bubbled with air containing 390 ppmv or 750 ppmv CO_2. Increased pCO_2 led to increased growth rates in all three strains. In addition, protein levels of RUBISCO increased in the coastal strains of both species, showing a larger capacity for CO_2 assimilation at 750 ppmv CO_2. With increased pCO_2, both *T. pseudonana* strains displayed an increased susceptibility to PSII photoinactivation and, to compensate, an augmented capacity for PSII repair. Consequently, the cost of maintaining PSII function for the diatoms increased at increased pCO_2. In *E. huxleyi*, PSII photoinactivation and the counteracting repair, while both intrinsically larger than in *T. pseudonana*, did not change between the current and high-pCO_2 treatments. The content of the photosynthetic electron transport intermediary cytochrome b6/f complex increased significantly in the diatoms under elevated pCO_2, suggesting changes in electron transport function.

Key index words: **cytochrome b6f; electron transport; *Emiliania huxleyi*; growth rate; ocean acidification; pCO_2; pH; photoinhibition; RUBISCO; *Thalassiosira pseudonana***

Abbreviations: **CCMs, carbon concentrating mechanisms; CCMP, Provasoli-Guillard National Center for the Culture of Marine Phytoplankton; $CO_{2(aq)}$, dissolved CO_2; DCMU, 3-(3,4-dichlorophenyl)-1,1-dimethylurea; DIC, dissolved inorganic carbon; EASW, enriched artificial seawater; ETR, electron transport rate; FIRe, fluorescence induction and relaxation; $F_{M\ DARK}$, maximum fluorescence in the dark-adapted state; $F_{M\ DCMU}$, maximal fluorescence in the presence of DCMU; F_M', maximum fluorescence in the light-adapted state; F_O, minimum fluorescence in the dark-adapted state; F_O', minimum fluorescence in the light-adapted state; F_S, steady-state fluorescence in the light-adapted state; F_V, variable fluorescence; K_M, half-saturation constant; NPQ, nonphotochemical quenching; pCO_2, partial pressure of CO_2; q_L, photochemical quenching; R_{PSII}, PSII repair rate; TA, total alkalinity; σ_I, effective absorption cross section for photons driving PSII photoinactivation; σ_{PSII}, the functional absorption cross section serving PSII photochemistry; $\Omega_{calcite}$, calcite saturation state**

For the past 10 million years, the atmospheric partial pressure of CO_2 (pCO_2) remained below 300 ppmv (Berner 1990, Pearson and Palmer 2000), but since the Industrial Revolution anthropogenic CO_2 has raised pCO_2 to 390 ppmv, and pCO_2 is projected to reach ~750 ppmv by the year 2100 (Houghton et al. 2001). The atmosphere and the surface ocean exchange CO_2 on time scales of several months (Zeebe and Wolf-Gladrow 2001), so increases in atmospheric pCO_2 lead to increases in oceanic dissolved CO_2 ($CO_{2\ (aq)}$), bicarbonate, and hydrogen ion concentrations, but decreases in carbonate ion concentrations (Caldeira and Wickett 2005). Furthermore, the concentrations and bioavailabilities of ammonia, ammonium, iron, phosphate, silicate, and toxins will be affected through pH-dependent speciation and solubility (Zeebe and Wolf-Gladrow 2001). Although these predicted changes in seawater chemistry are well described, the effects on marine organisms and ecosystems are not as clear. The responses of phytoplankton to changing seawater chemistry may vary among taxa,

[1]Received 4 July 2011. Accepted 8 December 2011.
[2]Present address: Department of Biology, Biological & Geological Sciences Building, University of Western Ontario, London, Ontario, Canada N6A 5B7.
[3]Author for correspondence: e-mail dcampbell@mta.ca.

which have divergent nutrient uptakes and metabolic resource allocations (Quigg et al. 2003).

Diatoms are responsible for ~40% of current marine primary productivity (Field et al. 1998) and tend to dominate the phytoplankton assemblage under nutrient-rich conditions, especially in turbulent coastal waters with fluctuating light (Macintyre et al. 2000), in part because they show low susceptibility to photoinactivation compared to other phytoplankton (Key et al. 2010, Loebl et al. 2010). In comparison to other phytoplankton, diatoms have a high efficiency of carbon sequestration into the deep ocean as their heavy silica frustules enhance sinking rates (Smetacek 1999). They have a form ID RUBISCO with greater CO_2/O_2 selectivity, but a lower half-saturation constant (K_M) than many other algae (Badger et al. 1998, Tcherkez et al. 2006). Both current and predicted future seawater $CO_{2\ (aq)}$ concentrations are well below the levels required to saturate their isolated RUBISCO enzyme (Rost and Riebesell 2004). However, many diatoms, especially bloom-forming ones, have active carbon concentrating mechanisms (CCMs) (Burkhardt et al. 2001) to accumulate both CO_2 and bicarbonate for photosynthesis (Satoh et al. 2001, Colman et al. 2002, Morel et al. 2002, Badger 2003). As $CO_{2\ (aq)}$ and bicarbonate concentrations rise, diatoms could derive net benefits through down-regulation of their CCMs, freeing resources for other biological processes. In the diatom *Phaeodactylum tricornutum* growth is indeed stimulated at the predicted future CO_2 concentration of 750 ppmv (Wu et al. 2010). Furthermore, increased CO_2 concentrations caused shifts in the dominance of diatom species in the phytoplankton assemblage of the Equatorial Pacific (Tortell et al. 2002), and of the Southern Ocean (Tortell et al. 2008).

Coccolithophores are another group of globally distributed phytoplankton which form extensive blooms in the current ocean. The coccolithophores are major calcifiers in the ocean because they produce calcium carbonate scales termed coccoliths, which cover the cell (Baumann et al. 2004). Coccolithophores have been a focus for studies on phytoplankton responses to increased pCO_2, as their calcification shows sensitivity to pH (Riebesell et al. 2000). Predicted drops in seawater carbonate concentrations will decrease in the saturation states of aragonite and calcite ($\Omega_{calcite}$), which could negatively affect calcification in coccolithophores (Morse et al. 2007). In early studies the coccolithophores *Emiliania huxleyi* and *Gephyrocapsa oceanica* displayed decreased calcification rates with increasing pCO_2 (Riebesell et al. 2000, Zondervan et al. 2001). This drop in calcification rate was hypothesized to decrease their competitiveness. Similar responses of decreased calcification under elevated pCO_2 were shown in a number of subsequent studies both in cultures (Zondervan et al. 2001, Sciandra et al. 2003), and in mesocosms (Delille et al. 2005, Engel et al. 2005). Another study, however, showed the opposite trend with calcification in *E. huxleyi* increasing under the future ocean, elevated pCO_2 scenario (Iglesias-Rodriguez et al. 2008). Calcification in two larger, heavily calcifying coccolithophore species (Langer et al. 2006) showed an optimum curve with CO_2 (*C. leptoporus*) but insensitivity to CO_2 in *C. pelagicus*. Coccolithophores possess a form ID RUBISCO and the cells have HCO_3^- channels (Herfort et al. 2002). Nevertheless, current $CO_{2\ (aq)}$ concentrations are not saturating for photosynthesis in *E. huxleyi* (Rost and Riebesell 2004), which could thus benefit from greater $CO_{2\ (aq)}$ concentrations.

The sensitivity of phytoplankton to variable light could also change under increased pCO_2. Photoinhibition in the diatom *Phaeodactylum tricornutum* increased under elevated pCO_2 (Wu et al. 2010). This increase in photoinhibition could potentially result from an increase in the photoinactivation rate, a decrease in the counteracting PSII repair rate, changes in the functional absorption cross section serving PSII, changes in pigment content or cellular optics, or changes in downstream metabolism that feedback to alter electron transfer or reactive oxygen activities associated with PSII. *E. huxleyi* inherently experiences faster photoinactivation and operates counteracting PSII repair at a faster rate than diatoms (Ragni et al. 2008, Loebl et al. 2010) and may therefore show distinct photophysiological responses to increased pCO_2. Photoinactivation of PSII is primarily affected by irradiance levels and cellular optics, whereas PSII repair is a metabolic process (Nishiyama et al. 2006) and is therefore affected by a variety of factors. A well-regulated PSII repair rate allows cells to endure or exploit rapid increases in light that occur when they are mixed up the water column to greater irradiance, while not expending excessive energy on rapid PSII repair when it is unnecessary. PSII function underlies photosynthetic productivity, and the continual PSII repair cycle is a major factor in differential phytoplankton responses to the environment (Six et al. 2007). We therefore used turbidostat treatments of representative marine centric diatoms and a coccolithophore, to determine if increased pCO_2 provokes differential changes in their photophysiology.

MATERIALS AND METHODS

Culture conditions. *E. huxleyi* isolated from the North Sea coast at Bergen, Norway was provided by the Alfred Wegener Institute for Polar and Marine Research in Germany. In addition, two strains of *T. pseudonana* were obtained from the Provasoli-Guillard National Center for Culture of Marine Phytoplankton (CCMP). *T. pseudonana* CCMP1014 was isolated from an offshore location in the North Pacific gyre and *T. pseudonana* CCMP 1335 was isolated from coastal Moriches Bay, New York, USA. Independently innoculated replicate cultures of each strain were grown in FMT-150 photobioreactors (Photon Systems Instruments, Drasov, Czech Republic) at 18.0°C in enriched artificial seawater (EASW) prepared following Berges et al. (2001) except with 54.5 μM Si and 0.82 mM

Sr. The cuvettes of the photobioreactor were cleaned, autoclaved and reinnoculated prior to each replicate growth experiment. Growth irradiance of 30 μmol·photons·m^{-2} ·s^{-1} (24:0 light:dark) was provided by a panel of blue light-emitting diodes (LEDs) and measured using a microspherical quantum sensor (US-SQS, Waltz, Germany). We grew the cultures at low, limiting light intensity to approximate growth near the bottom of the photic zone, to then assess their susceptibility to photoinactivation and PSII repair capacity through a shift to a greater light intensity simulating an vertical mixing event to upper regions of the photic zone. Growth light was even through the culture volume because the bioreactor cuvette inner volume is only ~2 cm thick and the LED illumination panel evenly covers the entire rear face of the cuvette. Cultures were grown in turbidostat mode, with frequent small rounds of dilution with pre-bubbled media delivered by an automated peristaltic pump to maintain density in the range of 30–45 nmol chl $a \cdot L^{-1}$ for *E. huxleyi* and *T. pseudonana* CCMP 1335, and 45–65 nmol chl $a \cdot L^{-1}$ for *T. pseudonana* CCMP 1014.

Control and analysis of the carbonate system. The seawater carbonate system was controlled by continuously aerating the cultures with a curtain of fine bubbles of air containing 390 or 750 ppmv CO_2 and emitted from four fine apertures in a gas line running across the bottom of the cuvette volume, at 500 mL · min^{-1}. The bubbling did not disrupt the growth (Shi et al. 2009) of our study species. Each replicate culture was grown for 7.5 generations at the treatment CO_2 level, with continuous logging of pH to verify the stability of the carbonate system. At the end of the growth period photophysiological parameters were measured, cell counts were performed, dissolved inorganic carbon (DIC) was determined, and samples of the culture were filtered and frozen for pigment, protein, and elemental analysis.

Ambient (2010) CO_2 treatment of 390 ppmv was provided by bubbling cultures with outdoor air (Sackville, New Brunswick, Canada; March 2009 to March 2010). Periodic measures of this ambient air showed only small variations in CO_2. The high CO_2 treatment of 750 ppmv was obtained by supplementing this airstream with 99.99% CO_2 using 16 series mass flow controllers (Qubit systems, Kingston, Ontario, Canada; factory calibrated 05/11/2009). The outdoor air was dried with a condensing chamber, mixed with supplemental CO_2 if necessary, filtered through a 0.2 μm effective pore size glass fiber filter (Millipore, Billerica, MA, USA), and then rehumidified prior to bubbling both the media reservoir and the culture bioreactor cuvette. In addition to bubbling the culture, the frequent turbidostat dilutions of the culture (see growth rates, below) with pre-bubbled media further stabilized the carbonate system in the face of potential draw-down of DIC by slow culture growth. We verified the performance of CO_2 control by comparing the target CO_2 levels to the pCO_2 achieved in the cultures (next paragraph).

pH measurements were made with InPro 325x glass electrodes (Mettler-Toledo, Columbus, OH, USA) in each of three separate bioreactor units. National Institute of Standards and Technology (NIST) buffers of pH 7.00 and 10.00 were used to calibrate the electrodes (Sigma-Aldrich, St. Louis, MO, USA). Culture pH was measured continuously throughout the growth period to detect any drift in the carbonate system; a few culture replicates that showed drift were stopped and excluded from further analyses. DIC was measured following McGinn et al. (2005). We used the standard program CO2SYS (Lewis and Wallace 1998) with NIST scale constants from Peng et al. (1987); K1, K2 from Mehrbach et al. (1973) to calculate total alkalinity, the calcite saturation state, and concentrations of $CO_{2\ (aq)}$, bicarbonate and carbonate, on the basis of measured temperature (18°C), salinity (35 g · L^{-1}), pH, DIC and the phosphate (21 μmol · L^{-1}), and silica (52.5 μmol · L^{-1}) concentrations of the prepared EASW.

Growth rates. Prior to the experiments, preliminary growth curves were obtained for each species, at each CO_2 level, by operating the bioreactors in batch mode. These preliminary growth curves were used to find a turbidostat set-point to maintain cells near the minimum detectable density where they were growing exponentially in this system. Following these preliminary tests, the reactor components were reautoclaved prior to each culture replicate grown in turbidostat mode.

Following each inoculation of the 400 mL cuvette, each culture replicate was grown without dilution for one to two generations until a density of ~45 nmol chl $a \cdot L^{-1}$ was achieved. Basal fluorescence level (F_O) was then used to monitor culture density continuously. Each culture replicate was then set to turbidostat mode to maintain this density by diluting the 400 mL culture with a 10% volumetric addition of pre-bubbled media by activation of a peristaltic pump when F_O reached a threshold value. Each continuous turbidostat culture replicate grew until its individual 3.5 L reservoir of EASW was depleted; therefore the duration of each culture replicate was ~7.5 generations of growth. Data from the cycles of growth and dilution from the last 80 h of each culture growth replicate were used to calculate growth rates, by fitting the rate of increase of F_O between turbidostat dilutions with exponential regressions.

Fluorescence induction and relaxation (FIRe) fluorometry. The functional absorption cross section serving PSII photochemistry (σ_{PSII}, $m^2 \cdot quanta^{-1}$) for blue light was determined using a single turnover flash method, using a FIRe fluorometer (Satlantic, Halifax, Nova Scotia, Canada). Samples from each culture replicate were dark adapted for 5 min and then treated with 2 min of 0, 30, or 450 μmol blue photons · m^{-2} · s^{-1}. After each light treatment, an 80 μs single turnover flash (blue LED 455 ± 2 nm) was then triggered, to saturate PSII photochemistry and to drive fluorescence to a maximum. The rise in fluorescence yield was analyzed using FIReWORX software (Barnett 2007). Absolute values of σ_{PSII} were determined using the flash irradiance calibration factors provided by Satlantic.

Variable fluorescence measurements. Samples (2 mL) from each culture replicate were dark adapted for 5 min in a temperature-controlled cuvette holder at 18°C. A blue-green modulated measuring light (4Hz; Xenon-PAM, Waltz, Effeltrich, Germany) was applied to the dark-adapted sample to measure F_O, then a saturating light pulse (4,000 μmol photons · m^{-2} · s^{-1}, 600 ms) was triggered to measure the maximal fluorescence level in the dark ($F_{M\ DARK}$). Subsequently, an actinic light was activated (450 μmol photons · m^{-2} · s^{-1}) for 1–3 min until the signal stabilized at F_S level. A second saturating light pulse was triggered to determine the light-acclimated maximal fluorescence at 450 μmol photons · m^{-2} · s^{-1} (F_M'). Then a dark period of 2 s was applied to measure the basal fluorescence level in light-acclimated sample, F_O'. A quantity of 20 mL of 1.0 mM 3-(3,4-dichlorophenyl)-1,1-dimethylurea (DCMU; Sigma-Aldrich) was then added to the cuvette and after signal stabilization, a saturating light pulse was triggered to determine the maximal fluorescence in the presence of DCMU ($F_{M\ DCMU}$). The photochemical yield of PSII was calculated as in equation 1, where F_M is the maximum fluorescence given by the largest of $F_{M\ DARK}$ or $F_{M\ DCMU}$.

$$F_V/F_M = (F_M - F_O)/F_M \quad (1)$$

Photochemical quenching (q_L), an index of the instantaneous fraction of PSII centers open for photochemistry was estimated as equation 2. Nonphotochemical quenching (NPQ) was estimated as the quenched fraction of maximal fluorescence as equation 3.

$$q_L = (F'_M - F_S)/(F'_M - F'_O) \times (F'_O/F_S) \quad (2)$$

$$NPQ = (F_M - F'_M)/F'_M \quad (3)$$

Electron transport rate (ETR) was estimated from the rate of electron generation from PSII light capture (eq. 4). PsbD (molecules PsbD · cell^{-1}), was used as a proxy for the number of PSII centers in these low-light grown cells. PsbD · cell^{-1} was multiplied by q_L to obtain the number of open PSII centers. The product of molecules PsbD · cell^{-1}, q_L and σ_{PSII} (m^2 · quanta^{-1}) then gave an estimate of total functional absorption cross section of all the open reaction centers in the cell. Multiplying through by PPFD (quanta · m^{-2} · s^{-1}), gave an estimate of the cellular PSII electron generation rate (electrons · s^{-1} · cell^{-1}).

$$ETR = \sigma_{PSII} \times PsbD \times q_L \times PPFD \quad (4)$$

Light stress and recovery experiments. A light shift experiment was conducted with 130 mL taken from each culture growth replicate to determine the effective absorption cross section for photons driving PSII photoinactivation (σ_I) and the PSII repair rate. The culture sample was divided into two flasks and one was supplemented with 500 μg · mL^{-1} lincomycin (Sigma-Aldrich) to inhibit chloroplast ribosome function (Key et al. 2010, Loebl et al. 2010, Wu et al. 2011) and to thereby block PSII repair by blocking replacement of protein subunits, in particular the PsbA subunit which is subject to photoinactivation. The lincomycin stock solution was titrated to the culture pH prior to use to avoid perturbing the culture pH. Both flasks were placed in the dark for 10 min to allow the antibiotic to penetrate the cells and inhibit ribosome function. The flasks were then shifted to 450 μmol photons · m^{-2} · s^{-1} blue light (LEE Filter #183, Panavision; 455–479 nm peak transmission, 406–529 nm half-height width). Quantities of 2 mL samples were collected from both flasks at 15 min intervals over 90 min for XePAM measurements. A 1 h recovery phase followed the high-light shift, with the flasks returned to their growth irradiance level of 30 μmol photons · m^{-2} · s^{-1} blue light.

The exponential decrease in F_V/F_M in the lincomycin inhibited flask versus cumulative photons was fit to obtain σ_I (m^2 · quanta^{-1}) (eq. 5) (Oliver et al. 2003, Six et al. 2007, Campbell and Tyystjärvi 2011), a target size formulation that expresses the cellular susceptibility to photoinactivation of PSII, on the basis of incident light. The rate of photoinactivation at growth light (30 μmol photons · m^{-2} · s^{-1}) is given by the product of σ_I (m^2 · quanta^{-1}), the applied PPFD (quanta · m^{-2} · s^{-1}), the concentration of PsbA (molecules PsbA · μm^{-3}), and the fraction of PsbA which were serving in PSII centers, P, which was estimated separately as 0.95–0.99. Since there was no net photoinhibition observed at the low growth light, the rate of photoinactivation and PSII repair (R_{PSII}) were equal, allowing the magnitude of R_{PSII} to be calculated estimated as shown in equation 6.

$$[F_V/F_M]_t = [F_V/F_M]_0^{e^{\sigma_1 E_t}} \quad (5)$$

$$R_{PSII} = \sigma_I \times PPFD \times [PsbA] \times P \quad (6)$$

Elemental analysis. A 35 mL sample from each culture replicate was filtered onto a 13 mm glass fiber filter, which had been precombusted 5 h at 520°C, and then immediately frozen at −80°C. Filters carrying *E. huxleyi* were fumed in precombusted glassware with 30% HCl for 6 h prior to drying to drive off the carbonate content of the liths. All filters were dried at 55°C for 12 h prior to analysis. Nitrogen and carbon content of all *T. pseudonana* samples were determined using a Vario EL III Elemental Analyzer (Elementar, Hanau, Germany).

Pigment analysis. Quantities of 20 mL samples from each culture replicate were filtered onto 25 mm glass fiber filters, flash frozen in liquid nitrogen, and stored at −80°C. Pigments were extracted in the dark in methanol, and separated using high-performance liquid chromatography (Zapata et al. 2000). Pigments were identified according to their retention time and spectrum, and quantified by comparison with standards (Danish Hydraulic Institute [DHI], http://c14.dhigroup.com). Trans-β-Apo-8′-carotenal was used as an internal standard.

Protein analysis. Quantities of 50 mL samples from each culture replicate were filtered onto 25 mm glass fiber filters, flash frozen in liquid nitrogen, and stored at −80°C. These samples were later analyzed via quantitative immunoblotting (Six et al. 2007, Brown et al. 2008) to determine molar levels of PsbA, PsbD, PsaC, PetC, and RbcL.

Data analysis. Multivariate analyses of variance (MANOVAs) were used to assess whether CO_2 and/or species had a significant overall effect on the dependent parameters. Mean substitution was used to substitute missing data for MANOVA analyses only. Two-way analyses of variance (ANOVAs) were then used to test the effects of species and pCO_2 on each individual dependent variable. The SPSS software package was used for all statistical calculations (SPSS Inc 2008).

RESULTS

The applied pCO_2 treatment had the expected significant effect ($P \leq 0.001$) on achieved pCO_2, pH, $\Omega_{calcite}$, and on concentrations of bicarbonate, carbonate, and $CO_{2\ (aq)}$. The changes we observed are similar to those achieved in open system CO_2 perturbation experiments (Rost et al. 2008), and as seen in Fig. 1 they closely match the changes that

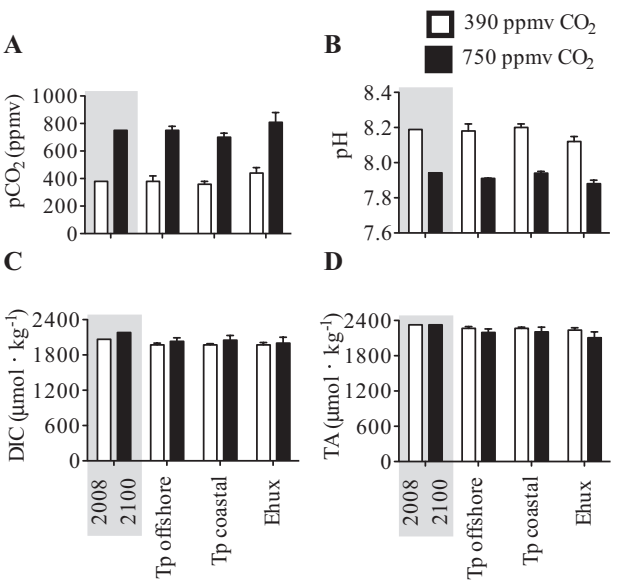

FIG. 1. The carbonate system in the photobioreactors, in comparison to ocean seawater chemistry for current (year 2008) and future (year 2100) projections. (A) Partial pressure of carbon dioxide (pCO_2), (B) pH, (C) dissolved inorganic carbon (DIC), and (D) total alkalinity (TA). *Thalassiosira pseudonana* CCMP1014 (Tp offshore, $n = 3$), *T. pseudonana* CCMP1335 (Tp coastal, $n = 4$), *Emiliania huxleyi* (Ehux, $n = 4$). Error bars represent standard deviation.

are predicted to occur to seawater chemistry over the next 90 years. There was also a small but statistically significant effect of pCO_2 treatment on calculated TA ($P = 0.031$, partial $\eta^2 = 0.26$), which was 2%–6% lower under 750 ppmv pCO_2. We suspect this unexpected decrease in TA with pCO_2 is a minor artifact of the CO2SYS calculations, because all the cultures were growing and continuously diluted with EASW media of the same alkalinity. The values of pCO_2 calculated from analytical pH and DIC measurements were close to the target pCO_2 levels set by the gas mass flow controllers, demonstrating that the biological activity of these slowly growing cultures had a minimal effect on the seawater carbonate chemistry, which was essentially controlled by the culture bubbling and the turbidostat dilutions with fresh, pre-bubbled media. The details of the carbonate system achieved in the photobioreactors are shown in Table 1 to facilitate comparisons with other studies.

A two-way ANOVA revealed that across all species there was a significant increase in growth rate under elevated pCO_2 ($P = 0.009$), (Fig. 2A). CO_2 thus had a fertilization effect on all species, enhancing growth rates 20%–40%, at least under these culture conditions of nutrient repletion and low, constant growth light. There was also a significant effect of species on growth rate ($P = 0.008$), with the offshore strain of *T. pseudonana* having a lower growth rate than the coastal strains of both *T. pseudonana* and *E. huxleyi* (Fig. 2A). There was no significant effect of elevated pCO_2 on cellular chl *a* content (Fig. 2B) nor on cell volume (Table 2), although we measured only cell volume and not organic cell volume, so we were not able to disentangle possible changes to organic cell volume from possible counteracting changes to the size of the *E. huxleyi* coccolith or diatom frustule layer.

σ_I, the susceptibility to photoinactivation of PSII, was significantly affected by pCO_2 ($P = 0.031$, Fig. 3A) and species ($P < 0.001$). Increased pCO_2 leads to increased σ_I in both the offshore *T. pseudonana* strain whose σ_I increased from 3.4×10^{-5} to 4.8×10^{-5} $A^2 \cdot quanta^{-1}$ and in the coastal *T. pseudonana* strain whose σ_I increased from 2.9×10^{-5} to 4.5×10^{-5} $A^2 \cdot quanta^{-1}$. In contrast, *E. huxleyi* displays a larger σ_I of 1.2×10^{-4} $A^2 \cdot quanta^{-1}$, but this susceptibility to photoinactivation of PSII did not change between the current and increased pCO_2 treatments. R_{PSII} operated at rates sufficient to completely counteract photoinactivation in all species at the growth light, since no net photoinhibition was

TABLE 1. Parameters detailing the seawater carbonate system of all culture replicates. Dissolved inorganic carbon (DIC) and pH were measured analytically at the end of growth of all ambient (390 ppmv CO_2) and high (750 ppmv CO_2) culture replicates. A full description of the carbonate system was calculated from temperature (18°C), salinity (35 $g \cdot L^{-1}$), pH, and the concentrations of DIC, phosphate (21 $\mu mol \cdot L^{-1}$), and silica (52.5 $\mu mol \cdot L^{-1}$) using the DOS program CO2SYS (Lewis and Wallace 1998).

			Measured analytically		Calculated with CO2SYS				
Species	Target pCO_2 treatment	Rep	DIC [$\mu mol \cdot kg^{-1}$]	pH (NIST)	pCO_2 [ppmv]	TA [$\mu mol \cdot kg^{-1}$]	HCO_3^- [$\mu mol \cdot kg^{-1}$]	CO_3^{2-} [$\mu mol \cdot kg^{-1}$]	CO_2 [$\mu mol \cdot kg^{-1}$]
Thalassiosira pseudonana (offshore)	390 ppmv	1	1,943	8.22	341	2,250	1,754	178	12
		2	1,975	8.14	416	2,243	1,806	155	14
		3	2,001	8.19	377	2,296	1,816	172	13
		AV±SD	1,970 ± 30	8.18 ± 0.04	380 ± 40	2,260 ± 30	1,790 ± 30	170 ± 10	13 ± 1
	750 ppmv	1	2,098	7.91	779	2,265	1,973	98	27
		2	1,994	7.91	732	2,159	1,875	94	25
		3	1,989	7.91	731	2,154	1,870	94	25
		AV±SD	2,030 ± 60	7.91 ± 0.002	750 ± 30	2,190 ± 60	1,910 ± 60	96 ± 2	26 ± 1
Thalassiosira pseudonana (coastal)	390 ppmv	1	1,940	8.22	333	2,252	1,748	181	11
		2	1,954	8.20	357	2,252	1,769	173	12
		3	1,970	8.17	388	2,252	1,794	163	13
		4	1,997	8.20	361	2,301	1,806	178	12
		AV±SD	1,970 ± 20	8.20 ± 0.02	360 ± 20	2,260 ± 20	1,780 ± 30	174 ± 8	12 ± 1
	750 ppmv	1	2,156	7.95	724	2,343	2,021	111	25
		2	2,005	7.92	713	2,176	1,883	98	25
		3	2,044	7.94	701	2,223	1,917	103	24
		4	1,972	7.96	650	2,154	1,847	103	22
		AV±SD	2,050 ± 80	7.94 ± 0.01	700 ± 30	2,220 ± 80	1,920 ± 80	104 ± 5	24 ± 1
Emiliania huxleyi	390 ppmv	1	2,007	8.09	477	2,252	1,850	141	16
		2	1,914	8.15	390	2,184	1,747	154	13
		3	1,973	8.11	446	2,226	1,813	145	15
		4	2,000	8.13	434	2,263	1,833	152	15
		AV±SD	1,970 ± 40	8.12 ± 0.03	440 ± 40	2,230 ± 40	1,810 ± 50	148 ± 6	15 ± 1
	750 ppmv	1	2,082	7.85	888	2,226	1,966	86	30
		2	2,084	7.87	845	2,236	1,965	90	29
		3	1,894	7.89	739	2,047	1,784	85	25
		4	1,932	7.88	767	2,083	1,821	85	26
		AV±SD	2,000 ± 100	7.88 ± 0.02	810 ± 70	2,100 ± 100	1,900 ± 100	87 ± 2	27 ± 2

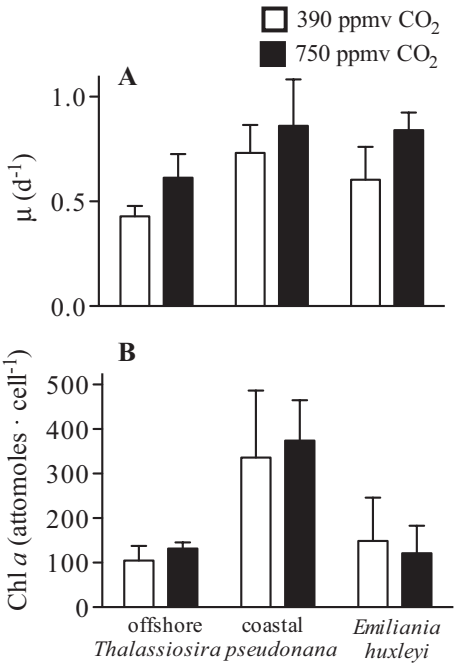

FIG. 2. The effect of partial pressure of carbon dioxide on (A) specific growth rate (μ) and (B) cellular chl *a* content (chl *a* ·cell^{-1}). Error bars represent standard deviation ($n = 3$ for the offshore strain of *Thalassiosira pseudonana* [CCMP 1014], $n = 4$ for the coastal strain of *T. pseudonana* [CCMP1335], and $n = 4$ for *Emiliania huxleyi*).

observed in the control cultures not treated with lincomycin.

σ_{PSII} ($A^2 \cdot$ quanta^{-1}, ±SD, Fig. 3C), the effective absorbance cross section for PSII photochemistry, shows no change with pCO_2 ($P = 0.356$). There is, however, a significant effect of species ($P = 0.001$). The offshore and coastal diatom strains have similar values of σ_{PSII} of 296 (± 10) and 289 (± 4) $A^2 \cdot$ quanta^{-1}, while *E. huxleyi* has a somewhat larger σ_{PSII} of 360 (±10) $A^2 \cdot$ quanta^{-1}. The ratio of σ_{PSII}/σ_I (Fig. 3D) gives the unitless ratio of excitons delivered to PSII to PSII photoinactivations. This ratio is $6.3–9.8 \times 10^6$ for *T. pseudonana* but is lower in *E. huxleyi* at 3.0×10^6. For *T. pseudonana*, σ_{PSII}/σ_I decreased with increasing pCO_2, while the ratio showed no CO_2 sensitivity in *E. huxleyi*.

q_L measured at 450 μmol photons · m^{-2} · s^{-1}. q_L showed no significant variation with pCO_2 (Fig. 4A), but q_L did vary across species ($P < 0.001$). The offshore diatom strain had a q_L of 0.45 (± 0.02) while the coastal diatom strain showed a q_L of 0.31 (± 0.03). *E. huxleyi* had a lower q_L of 0.20 (± 0.02). NPQ, measured at 450 μmol photons · m^{-2} · s^{-1}, did not change with pCO_2 level ($P = 0.682$), but did, however, vary significantly across species ($P < 0.001$) (Table 3). The offshore diatom displayed a high NPQ of 0.93 (± 0.06), while the coastal diatom had an NPQ of 0.49 (± 0.06), and *E. huxleyi* had an NPQ 0.36 (± 0.04) at 450 μmol photons · m^{-2} · s^{-1}.

Pigment composition showed few significant differences between the two pCO_2 treatments (see Table 2). In addition, carbon · μm^{-3} and chl *a* · μm^{-3} were similar across all species. The offshore *T. pseudonana* strain had a cell volume of 18 ± 1 μm^3 (including frustule), the coastal *T. pseudonana* had a cell volume of 39 ± 9 μm^3 (including frustule), and *E. huxleyi* had a cell volume of 19 ± 2 μm^3 (including coccoliths) (Table 2). During 90 min of high-light shift, total xanthophyll pigment content increased by 55% in *E. huxleyi*, 88% in the offshore *T. pseudonana* strain, and 55% in the coastal *T. pseudonana* strain. The de-epoxidation ratios (diatoxanthin/diadinoxanthin), of *T. pseudonana* were initially 0.04 at growth light (30 μmol photons · m^{-2} · s^{-1}), and increased to 0.50 after 90 min at higher light (450 μmol photons · m^{-2} · s^{-1}). Similarly, de-epoxidation ratios in *E. huxleyi* increased from 0.09 to 0.53 after 90 min at higher light. The lincomycin treatment decreased the achieved de-epoxidation, suggesting that de-epoxidation relied upon continuing plastidic protein synthesis, and/or that loss of active PSII centers in the presence of lincomycin limited the progress of de-epoxidation.

Total cellular protein did not change between ambient and 750 ppmv CO_2 treatments (Table 2). In addition, pCO_2 did not have a significant effect on PSI (PsaC) nor PSII protein content (PsbD and PsbA). ANOVAs showed that pCO_2 did have significant effects on RUBISCO (RbcL, $P = 0.025$) and cytocrome b6/f (PetC, $P < 0.001$) protein levels (Table 2). Cellular RUBISCO content showed a 2- to 3-fold increase with pCO_2 in both *E. huxleyi* and in the coastal diatom strain (Fig. 5A). Cytochrome b6/f content increased 4-fold in the offshore diatom strain, and 2-fold in the coastal strain (Fig. 5B). An antibody reactive to PetC from Haptophytes was not available to us so PetC content in *E. huxleyi* was not measured.

MANOVAs were executed on all three groups of dependent variables: the carbonate system, growth/physiology, and pigment/protein. MANOVA results revealed that pCO_2 level had a significant effect on the dependent variables of the carbonate system, $F(8, 9) = 195.82$, $P < 0.001$, on dependent variables related to growth and physiology, $F(11, 6) = 6.70$, $P = 0.015$, and on pigment and protein levels, $F(10, 7) = 4.28$, $P = 0.033$. Furthermore, the MANOVA results also showed that species had a significant effect on the dependent variables of all three groups. Separate two-way ANOVAs were conducted to identify specific dependent variables that contributed to these significant overall effects (summarized in Table 3).

DISCUSSION

Following inoculation of the photobioreactors, the seawater carbonate system reached target values within a few hours, accurately simulating current

TABLE 2. Protein and pigment content of all species studied at both pCO_2 levels. Protein levels of major components of photosynthesis were measured: RUBISCO (RbcL), PSII reaction centers (PsbD and PsbA), PSI reaction centers (PsaC), and cytochrome b6/f (PetC). Pigment abbreviations: 19′-butanoyloxyfucoxanthin (BFU), 4-keto-19′-hexanoyloxyfucoxanthin (4k-hex-fuco), 19′-hexanoyloxyfucoxanthin (HFU). Standard error is shown in brackets (n = 3 for *Thalassiosira pseudonana* offshore, n = 4 for *Thalassiosira pseudonana* coastal, and n = 4 *Emiliania huxleyi*).

	Thalassiosira pseudonana offshore		*Thalassiosira pseudonana* coastal		*Emiliania huxleyi*	
	390 ppmv	750 ppmv	390 ppmv	750 ppmv	390 ppmv	750 ppmv
Carbon (pg ·cell^{-1})	4.6 (±0.8)	5.7 (±0.5)	15.4 (±3.6)	19.8 (±2.4)	20 (±10)	13 (±3)
C:N ratio	5.8 (±0.2)	5.2 (±0.5)	5.6 (±0.3)	5.3 (±0.4)	5.9 (±0.6)	5.6 (±0.2)
Total protein (μg ·cell^{-1})	2.2×10^{-6} ($\pm 0.6 \times 10^{-6}$)	3.4×10^{-6} ($\pm 0.4 \times 10^{-6}$)	2.4×10^{-5} ($\pm 0.8 \times 10^{-5}$)	6.8×10^{-6} ($\pm 0.5 \times 10^{-6}$)	1.0×10^{-5} ($\pm 0.1 \times 10^{-5}$)	1.0×10^{-5} ($\pm 0.2 \times 10^{-5}$)
Cell volume (μm^3)	17 (±1)	20 (±1)	50 (±10)	30 (±10)	20 (±3)	17 (±2)
Cell count (cells ·mL^{-1})	560,000 (±60,000)	360,000 (±50,000)	160,000 (±70,000)	200,000 (±90,000)	320,000 (±90,000)	340,000 (±60,000)
Protein (attomoles ·cell^{-1})						
PsbA	0.11 (±0.02)	0.16 (±0.01)	1.2 (±0.4)	0.8 (±0.1)	0.081 (±0.001)	0.053 (±0.009)
PsbD	0.25 (±0.06)	0.35 (±0.03)	0.8 (±0.2)	1.5 (±0.3)	0.48 (±0.08)	0.5 (±0.2)
PsaC	0.24 (±0.1)	0.25 (±0.02)	0.77 (±0.2)	0.4 (±0.2)	0.09 (±0.02)	0.06 (±0.02)
RbcL	3.7 (±0.7)	4.4 (±0.5)	6 (±2)	013 (±2)	0.20 (±0.07)	0.6 (±0.1)
PetC	0.17 (±0.04)	0.66 (±0.05)	0.38 (±0.08)	0.69 (±0.06)	–	–
Pigment (attomoles ·cell^{-1})						
Chl *a*	110 (±20)	131 (±8)	340 (±80)	370 (±50)	150 (±50)	120 (±30)
Chl *c*1	0.9 (±0.3)	0.8 (±0.1)	1 (±0.2)	1.2 (±0.8)	–	–
Chl *c*2	3.2 (±0.4)	3.7 (±0.2)	8 (±2)	13 (±3)	20 (±7)	16 (±4)
Chl *c*3	–	–	–	–	14 (±4)	12 (±4)
MV chl *c*3	–	–	–	–	3 (±1)	2 (±1)
BFU	–	–	–	–	0.4 (±0.2)	0.3 (±0.1)
Fucoxanthin	32 (±6)	41 (±3)	110 (±20)	120 (±20)	29 (±9)	22 (±7)
4k-hex-fuco	–	–	–	–	21 (±8)	14.8 (±5)
HFU	–	–	–	–	73 (±20)	67 (±20)
Diadinoxanthin	5 (±1)	6.1 (±0.3)	17 (±4)	15 (±2)	7 (±3)	7 (±1)
Diatoxanthin	0.03 (±0.03)	0.16 (±0.09)	2 (±1)	5 (±4)	1.1 (±0.8)	0.6 (±0.2)
β,β-carotene	2.2 (±0.4)	2.7 (±0.2)	6 (±1)	7.3 (±0.8)	1.8 (±0.6)	1.5 (±0.3)
β,ε-carotene	–	–	–	–	0.2 (±0.2)	0.6 (±0.3)

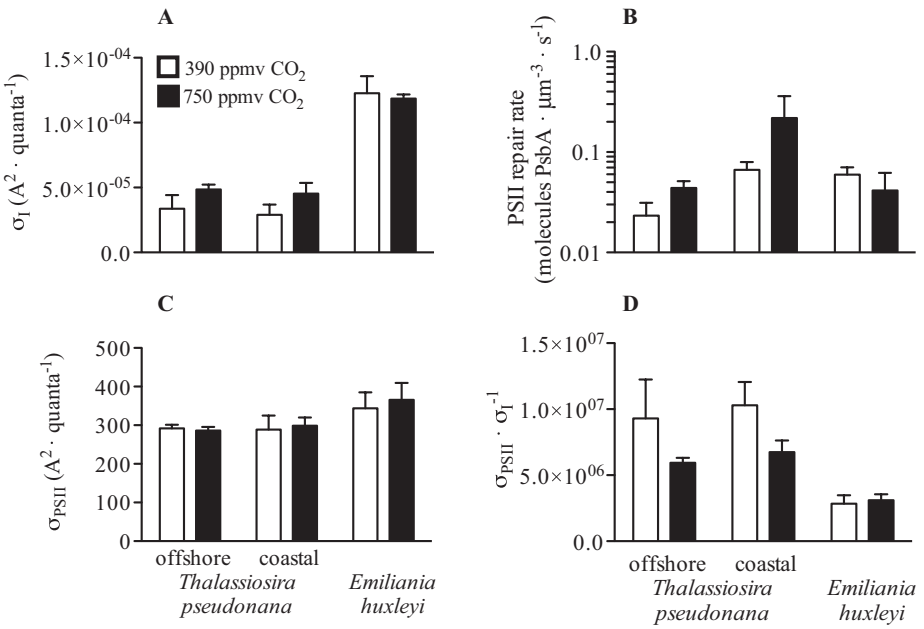

FIG. 3. The effect of partial pressure of carbon dioxide on (A) the effective absorption cross section for photons driving PSII photoinactivation (σ_I), (B) PSII repair rate, (C) the effective absorption cross section serving PSII photochemistry (σ_{PSII}), and (D) the ratio of σ_{PSII}/σ_I. PSII repair rate is displayed on a log axis. Error bars represent standard deviation (n = 3 for the offshore strain of *Thalassiosira pseudonana* [CCMP 1014], n = 4 for the coastal strain of *T. pseudonana* [CCMP1335], and n = 4 for *Emiliania huxleyi*).

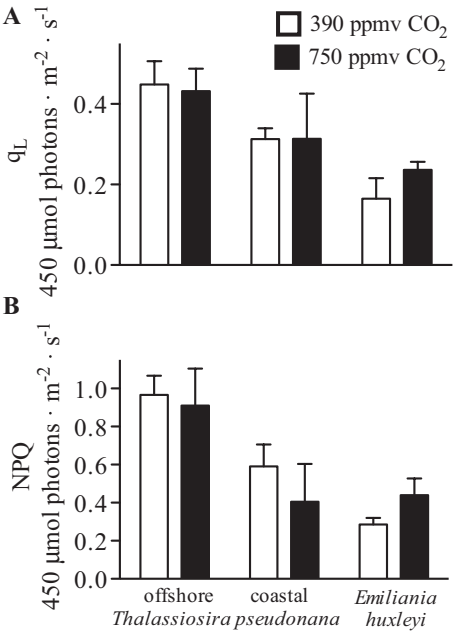

FIG. 4. The effect of partial pressure of carbon dioxide on (A) photochemical quenching (q_L) and (B) nonphotochemical quenching (NPQ). Error bars represent standard deviation ($n = 3$ for the offshore strain of *Thalassiosira pseudonana* [CCMP 1014], $n = 4$ for the coastal strain of *T. pseudonana* [CCMP1335], and $n = 4$ for *Emiliania huxleyi*).

(390 ppmv CO_2) or future conditions (750 ppmv CO_2). These conditions were narrowly maintained throughout the entire 7.5-generation treatment period. DIC was replenished through constant bubbling, and through frequent dilution with pre-bubbled culture media. The pH of the culture did not vary during growth and changes in TA were minimal. The biological activity from the slowly growing cultures therefore did not perturb the media chemistry sufficiently to outrun the stabilizing influences of gas bubbling and turbidostat media replenishment.

The 750 ppmv CO_2 treatments had a fertilization effect on the growth rates of *T. pseudonana* and *E. huxleyi* grown under low light and nutrient repletion. This could be due to the increased diffusive supply of CO_2, as both these species are relatively small in size. In addition, at greater CO_2 and bicarbonate concentrations, CCMs can be down-regulated, freeing resources for other metabolic activities such as increased growth rate. The increase in growth rate was not due to a decrease in cell size, as there was no significant change in total cell volume nor in chl *a* per cell. This enhanced growth rate observed at low light and nutrient repletion imparts these species with increased competitive ability under these conditions. Increased pCO_2 could therefore affect community composition, provided that all phytoplankton do not benefit to the same extent.

Increased pCO_2 also resulted in increased RUBISCO protein content in the coastal strains of both *T. pseudonana* and *E. huxleyi*, giving a greater potential capacity for CO_2 assimilation. The RUBISCO content of the offshore strain of *T. pseudonana* did not change between CO_2 levels, although it was inherently greater than the coastal strain when normalized to carbon content or biovolume. These results suggest that there could be a net increase in capacity for primary productivity at 750 ppmv CO_2, at least with regard to small diatoms and coccolithophores in coastal environments. However, these results may be limited to the low-light, high-nutrient conditions of this study.

When more CO_2 is available, *E. huxleyi* was able to increase growth rate without an increase in the rate of reductant generation through light capture (Fig. 6), and must therefore have achieved a greater metabolic conversion of generated reductant to accumulated biomass. We note that this effect is for cells growing under light limitation, where a metabolic reallocation that lowers the energy cost for growth can most readily manifest. The diatoms showed a different functional response, achieving an increased growth rate at 750 ppmv CO_2 in parallel with a commensurate increase in the rate of reductant generation.

Although photoinactivation was not sensitive to pCO_2 in *E. huxleyi*, both strains of *T. pseudonana* became more susceptible to photoinactivation at 750 ppmv CO_2 than at 390 ppmv CO_2. This is consistent with results from Wu et al. (2010) who showed increased photoinhibition in *P. tricornutum* at 750 ppmv CO_2. The increase in σ_I in diatoms under 750 ppmv CO_2 increased the cost of maintaining the PSII pool, particularly since the cellular PSII content was equivalent at current and elevated pCO_2. To maintain PSII function, every photoinactivation event must be countered by the PSII repair process. We indeed found that under 750 ppmv CO_2 R_{PSII} operated at an increased rate to cope with the increased photoinactivation rate. Therefore, in *T. pseudonana*, the metabolic cost of maintaining PSII function in high or fluctuating light scenarios was greater at 750 ppmv CO_2. This, however, did not result in a net negative impact on growth rate, under the experimental growth conditions of low, constant light and nutrient repletion. Future experiments should examine growth under fluctuating light or shifts to yet greater light levels to see if the maximum tolerable light level varies between pCO_2 treatments. Unless the repair capacity increases enough to counter the larger σ_I, the maximum tolerable light level or maximum tolerable duration of high light exposure will be lower at 750 ppmv CO_2. This phenomenon could have serious implications for these small diatoms, especially the coastal strains which are exposed to wider light fluctuations due to sharp attenuation of the light gradient and larger vertical mixing rates (Macintyre et al. 2000). The

TABLE 3. Table of two-way analysis of variance results. Partial pressure of CO_2 (pCO_2), dissolved inorganic carbon (DIC), total alkalinity (TA), the calcite saturation state ($\Omega_{calcite}$), specific growth rate (μ), the effective absorption cross section for photons driving photoinactivation of PSII (σ_I), PSII repair rate (R_{PSII}), the effective absorption cross section for photons driving photochemistry of PSII (σ_{PSII}), photochemical quenching (q_L), nonphotochemical quenching (NPQ), electron transport rate (ETR), RUBISCO protein (RbcL), PSII reaction centers protein (PsbD and PsbA), PSI reaction centers protein (PsaC), cytochrome b6/f protein (PetC), fucoxanthin (fuco), diadinoxanthin (diadino), and diatoxanthin (diato).

	pCO_2			Species			Interaction		
	F-value	df	*P*-value	*F*-value	df	*P*-value	*F*-value	df	*P*-value
Carbonate system									
pCO_2	412.127	1,16	<0.001	10.832	2,16	0.001	0.442	2,16	0.651
pH	775.547	1,16	<0.001	25.256	2,16	<0.001	0.311	2,16	0.737
DIC	0.015	1,16	0.903	0.603	2,16	0.559	0.652	2,16	0.534
TA	5.580	1,16	0.031	1.535	2,16	0.245	0.239	2,16	0.790
HCO_3^-	16.567	1,16	0.001	0.001	2,16	0.999	0.554	2,16	0.585
CO_3^{2-}	576.969	1,16	<0.001	21.995	2,16	<0.001	1.490	2,16	0.255
$CO_{2\ (aq)}$	390.510	1,16	<0.001	9.133	2,16	0.002	0.152	2,16	0.860
$\Omega_{calcite}$	600.856	1,16	<0.001	24.107	2,16	<0.001	1.589	2,16	0.235
Growth/physiology									
μ	8.953	1,16	0.009	6.605	2,16	0.008	0.284	2,16	0.756
σ_I	5.621	1,16	0.031	226.155	2,16	<0.001	3.334	2,16	0.062
R_{PSII}	3.650	1,16	0.074	6.547	2,16	0.008	3.988	2,16	0.039
σ_{PSII}	0.420	1,16	0.526	9.890	2,16	0.002	0.361	2,16	0.739
σ_{PSII}/σ_I	13.582	1,16	0.002	35.377	2,16	<0.001	4.490	2,16	0.028
q_L	0.475	1,16	0.500	25.530	2,16	<0.001	1.030	2,16	0.379
NPQ	0.174	1,16	0.682	32.248	2,16	<0.001	3.202	2,16	0.068
ETR	2.953	1,16	0.105	11.275	2,16	0.001	2.005	2,16	0.167
Cell volume	1.834	1,16	0.194	5.372	2,16	0.016	1.813	2,16	0.195
Total protein · $cell^{-1}$	2.002	1,14	0.179	4.267	2,14	0.036	3.014	2,14	0.301
Carbon $cell^{-1}$	0.253	1,16	0.622	2.636	2,16	0.102	0.743	2,16	0.492
Protein/pigment									
PsbA · $cell^{-1}$	0.541	1,13	0.475	13.158	2,13	0.001	0.738	2,13	0.497
PsbD · $cell^{-1}$	2.241	1,14	0.157	9.497	2,14	0.002	1.564	2,14	0.244
PsaC · $cell^{-1}$	1.063	1,14	0.320	7.897	2,14	0.005	1.056	2,14	0.374
RbcL · $cell^{-1}$	6.316	1,14	0.025	23.187	2,14	<0.001	4.658	2,14	0.028
*PetC · $cell^{-1}$	36.230	1,10	<0.001	3.255	1,10	0.101	1.833	1,10	0.206
Chl *a* · $cell^{-1}$	0.097	1,16	0.760	15.597	2,16	<0.001	0.287	2,16	0.754
*Chl *c*1 · $cell^{-1}$	0.786	1,10	0.396	9.296	1,10	0.012	1.483	1,10	0.251
Chl *c*2 · $cell^{-1}$	0.042	1,16	0.841	6.033	2,16	0.011	0.637	2,16	0.542
Fuco · $cell^{-1}$	0.320	1,16	0.580	25.339	2,16	<0.001	0.415	2,16	0.667
Diadino · $cell^{-1}$	0.129	1,16	0.724	10.664	2,16	0.001	0.309	2,16	0.739
Diato · $cell^{-1}$	0.314	1,16	0.583	1.547	2,16	0.243	0.473	2,16	0.632
β,β-carotene · $cell^{-1}$	0.382	1,16	0.545	25.207	2,16	<0.001	0.381	2,16	0.689

increased susceptibility to photoinactivation under increased pCO_2 thus impairs one of the key competitive advantages of diatoms over other phytoplankton when growing under variable light.

In contrast, in *E. huxleyi* σ_I and R_{PSII} did not change with pCO_2 level. *E. huxleyi* has a 2- to 3-fold greater susceptibility to photoinactivation compared to the diatoms. *E. huxleyi* also operated PSII repair at a much greater rate to counter this photoinactivation. Therefore, *E. huxleyi* expended more energy on PSII repair during photosynthesis, hence its lower σ_{PSII}/σ_I ratio, denoting a lower ratio of exciton delivery to photoinactivation events. These results confirm those of Ragni et al. (2008), and Loebl et al. (2010) who reported high rates of photoinactivation and repair in *E. huxleyi*, at least when growing under nutrient repletion. Despite the bigger metabolic cost of the PSII repair cycle, the growth rate of *E. huxleyi* is comparable to that of *T. pseudonana*, and the growth rate of *E. huxleyi* increased significantly with increased pCO_2.

In all species studied, there were no significant changes to the biochemical content of the PSI and PSII reaction centers nor antennae pigments between CO_2 treatments. In addition, σ_{PSII} showed no change with pCO_2. Therefore, the observed increase in growth rates in all species between CO_2 levels was not due to an increase in achieved light capture. Similarly, the increase in σ_I observed in the diatoms between CO_2 levels is not due to any detected change in the biochemical composition of the photosynthetic antennae nor reaction center content.

Both strains of diatoms showed increased cytochrome b6/f content at 750 ppmv CO_2. It remains to be seen whether cytochrome b6/f content in coccolithophores responds to changes in pCO_2 in the same manner. The increase in intersystem electron transport capacity may in part be helping the cells achieve the faster growth rates observed at 750 ppmv CO_2. The increased cytochrome b6/f content was, surprisingly, the most striking detected change

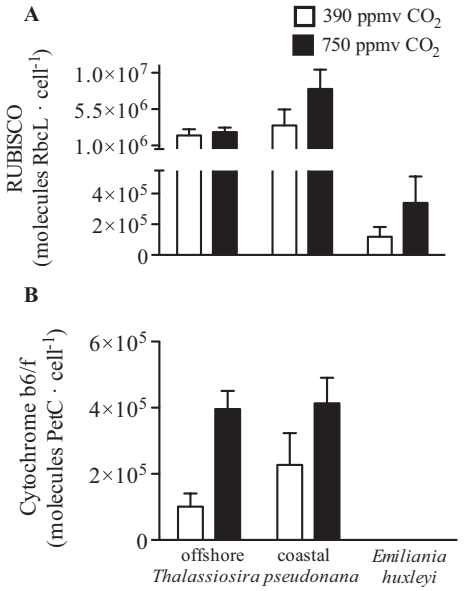

FIG. 5. (A) Cellular RUBISCO protein content and (B) cellular cytochrome b6/f protein content. The cellular protein content of RUBISCO and cytochrome b6/f was determined by measuring molar levels of RbcL and PetC via quantitative immunoblotting and normalizing to cell counts. Error bars represent standard deviation ($n = 3$ for the offshore strain of *Thalassiosira pseudonana* [CCMP 1014], $n = 4$ for the coastal strain of *T. pseudonana* [CCMP1335], and $n = 4$ for *Emiliania huxleyi*).

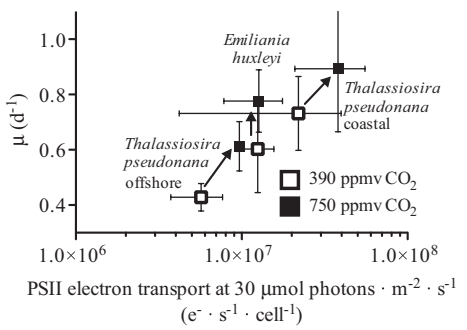

FIG. 6. The influence of pCO_2 on specific growth rate (μ) and cellular PSII electron transport rate. Arrows indicate the change from current to high pCO_2. Cellular PSII electron transport rate is displayed on a log axis. Error bars represent standard deviation ($n = 3$ for the offshore strain of *Thalassiosira pseudonana* [CCMP 1014], $n = 4$ for the coastal strain of *T. pseudonana* [CCMP1335], and $n = 4$ for *Emiliania huxleyi*).

in molecular composition in response to increased pCO_2, but the significance of the change remains obscure. We speculate that cytochrome b6/f content might be responding to changes in intracellular pH under increased pCO_2, which could provoke changes in the bioenergetics of proton and electron flux through the complex. The addition of isolated cytochrome b6/f complexes to a subthylakoid preparation of oxygen-evolving PSII core complexes enhances PSII photoinactivation, especially in response to blue and UV-A light (Suh et al. 2000). The chl cofactor of cytochrome b6/f is a probable site of photochemical $^1O_2$* generation that can provoke PSII photoinactivation (Sang et al. 2010). We speculate that the large increase in cytochrome b6/f content observed in the diatoms at 750 ppmv CO_2 could cause increased photogeneration of $^1O_2$*, thereby contributing to increased diatom PSII photoinactivation under 750 ppmv CO_2.

Coastal areas regularly experience greater natural fluctuations in the seawater carbonate system; we therefore expected increasing pCO_2 to have greater effects on the open-ocean strain than on the coastal strain. However, the ambient and high pCO_2 treatments had similar effects on both the coastal and open-ocean strains of *T. pseudonana*. It is possible that both these strains are well adapted to coping with the changes associated with changing pCO_2, as they are bloom forming species which occasionally experience comparable changes in seawater chemistry during blooms. Future experiments should examine non-bloom-forming species isolated from both coastal and offshore regions to see if their responses to pCO_2 differ. Some of the photophysiological parameters that were not CO_2 sensitive did differ inherently between the coastal and open-ocean strains. The open-ocean diatom showed more induction of NPQ than the coastal strain. These results show that the two strains have different strategies to deal with their respective light regimes.

This study details the effects of pCO_2 levels on growth rates, photophysiological parameters, and levels of key proteins and pigments of *T. pseudonana* and *E. huxleyi*. To our surprise, increasing pCO_2 provokes increased susceptibility to photoinactivation of PSII in diatoms, but not in the coccolithophore species, suggesting differential effects on these taxa under an increased future pCO_2. Diatoms currently thrive in variable light environments, in part through their low intrinsic susceptibility to photoinactivation. Under increased pCO_2 this competitive advantage may decrease.

We thank Yuelu Jiang of Texas A&M University at Galveston for the CHN analyses. We thank D. Hamilton of Mount Allison University for statistical consultation, Dr. Suzanne Roy of Université de Québec à Rimouski for hosting the analyses of pigmentation, and Dr. Benjamin Bailleul for stimulating discussions. Two anonymous reviewers, and the *Journal of Phycology* editor Dr. P. Thompson, provided extensive and constructive comments that helped us improve the manuscript. This work was funded by NSERC of Canada, Canada Research Chairs, the New Brunswick Innovation Foundation (D. A. C.) and a Mount Allison University Rice Graduate Fellowship (A. M.).

Badger, M. 2003. The roles of carbonic anhydrases in photosynthetic CO_2 concentrating mechanisms. *Photosynth. Res.* 77: 83–94.

Badger, M. R., Andrews, T. J., Whitney, S. M., Ludwig, M., Yellowlees, D. C., Leggat, W. & Price, G. D. 1998. The diversity and coevolution of Rubisco, plastids, pyrenoids, and chloroplast-based CO_2-concentrating mechanisms in algae. *Can. J. Bot. Rev. Can. Bot.* 76:1052–71.

Barnett, A. B. 2007. *Fireworx Version 1.0.4*. Available at: http://sourceforge.net/projects/fireworx (accessed 24 April 2012).

Baumann, K. H., Bockel, B. & Frenz, M. 2004. Coccolith contribution to south Atlantic carbonate sedimentation. *In* Thierstein, H. R. & Young, J. R. [Eds.] *Coccolithophores: From Molecular Processes to Global Impact*. Springer-Verlag, Berlin, pp. 367–402.

Berges, J. A., Franklin, D. J. & Harrison, P. J. 2001. Evolution of an artificial seawater medium: improvements in enriched seawater, artificial water over the last two decades. *J. Phycol.* 37:1138–45.

Berner, R. A. 1990. Atmospheric carbon-dioxide levels over Phanerozoic time. *Science* 249:1382–6.

Brown, C. M., Mackinnon, J. D., Cockshutt, A. M., Villareal, T. A. & Campbell, D. A. 2008. Flux capacities and acclimation costs in *Trichodesmium* from the Gulf of Mexico. *Mar. Biol.* 154:413–22.

Burkhardt, S., Amoroso, G., Riebesell, U. & Sultemeyer, D. 2001. CO_2 and HCO_3^- uptake in marine diatoms acclimated to different CO_2 concentrations. *Limnol. Oceanogr.* 46:1378–91.

Caldeira, K. & Wickett, M. E. 2005. Ocean model predictions of chemistry changes from carbon dioxide emissions to the atmosphere and ocean. *J. Geophys. Res. Oceans* 110: C09S04, DOI: 10.1029/2004JC002671.

Campbell, D. A. & Tyystjärvi, E. 2011. Parameterization of photosystem II photoinactivation and repair. *Biochim. Biophys. Acta* 1817:258–65.

Colman, B., Huertas, I. E., Bhatti, S. & Dason, J. S. 2002. The diversity of inorganic carbon acquisition mechanisms in eukaryotic microalgae. *Funct. Plant Biol.* 29:261–70.

Delille, B., Harlay, J., Zondervan, I., Jacquet, S., Chou, L., Wollast, R., Bellerby, R. G. J., Frankignoulle, M., Borges, A. V., Riebesell, U. & Gattuso, J. P. 2005. Response of primary production and calcification to changes of pCO_2 during experimental blooms of the coccolithophorid *Emiliania huxleyi*. *Glob. Biogeochem. Cycles* 19: GB2023, DOI: 10.1029/2004GB002318.

Engel, A., Zondervan, I., Aerts, K., Beaufort, L., Benthien, A., Chou, L., Delille, B., et al. 2005. Testing the direct effect of CO_2 concentration on a bloom of the coccolithophorid *Emiliania huxleyi* in mesocosm experiments. *Limnol. Oceanogr.* 50: 493–507.

Field, C. B., Behrenfeld, M. J., Randerson, J. T. & Falkowski, P. 1998. Primary production of the biosphere: integrating terrestrial and oceanic components. *Science* 281:237–40.

Herfort, L., Thanke, B. & Roberts, J. 2002. Acquisition and use of bicarbonate by *Emiliania huxleyi*. *New Phytol.* 156:427–36.

Houghton, J. T., Ding, Y., Griggs, D. J., Nouger, M., van der Linden, P. J., Dai, X., Maskell, K. & Johnson, C. A. 2001. *Climate Change 2001: The Scientific Basis. Contribution of Working Group I to the Third Assessment Report of the Intergovernmental Panel on Climate Change*. Cambridge University Press, New York, 881 pp.

Iglesias-Rodriguez, M. D., Halloran, P. R., Rickaby, R. E. M., Hall, I. R., Colmenero-Hidalgo, E., Gittins, J. R., Green, D. R. H. et al. 2008. Phytoplankton calcification in a high-CO_2 world. *Science* 320:336–40.

Key, T., McCarthy, A., Campbell, D. A., Six, C., Roy, S. & Finkel, Z. V. 2010. Cell size trade-offs govern light exploitation strategies in marine phytoplankton. *Environ. Microbiol.* 12:95–104.

Langer, G., Geisen, M., Baumann, K. H., Klas, J., Riebesell, U., Thoms, S. & Young, J. R. 2006. Species-specific responses of calcifying algae to changing seawater carbonate chemistry. *Geochem. Geophys. Geosystems* 7:Q09006, DOI: 10.1029/2005GC001227.

Lewis, E. & Wallace, D. W. R. 1998. *CO2SYS, Program Developed for CO_2 System Calculations ORNL/CDIAC-105*. Carbon Dioxide Information Analysis Center, Oak Ridge National Laboratory, U.S. Department of Energy, Oak Ridge, Tennessee.

Loebl, M., Cockshutt, A., Campbell, D. A. & Finkel, Z. V. 2010. Physiological basis for high resistance to photoinhibition under nitrogen depletion in *Emiliania huxleyi*. *Limnol. Oceanogr.* 55:2150–60.

Macintyre, H. L., Kana, T. M. & Geider, R. J. 2000. The effect of water motion on short-term rates of photosynthesis by marine phytoplankton. *Trends Plant Sci.* 5:12–7.

McGinn, P. J., Jones, M. J., Macdonald, A. B. & Campbell, D. A. 2005. Light is required for low-CO_2-mediated induction of transcripts encoding components of the CO_2-concentrating mechanism in the cyanobacterium *Synechococcus elongatus*: analysis by quantitative reverse transcription-polymerase chain reaction. *Can. J. Bot. Rev. Can. Bot.* 83:711–20.

Mehrbach, C., Culberson, C. H., Hawley, J. E. & Pytkowicz, R. M. 1973. Measurement of the apparent dissociation constants of carbonic acid in seawater at atmospheric pressure. *Limnol. Oceanogr.* 18:897–907.

Morel, F. M. M., Cox, E. H., Kraepiel, A. M. L., Lane, T. W., Milligan, A. J., Schaperdoth, I., Reinfelder, J. R. & Tortell, P. D. 2002. Acquisition of inorganic carbon by the marine diatom *Thalassiosira weissflogii*. *Funct. Plant Biol.* 29:301–8.

Morse, J. W., Arvidson, R. S. & Luttge, A. 2007. Calcium carbonate formation and dissolution. *Chem. Rev.* 107:342–81.

Nishiyama, Y., Allakhverdiev, S. I. & Murata, N. 2006. A new paradigm for the action of reactive oxygen species in the photoinhibition of photosystem II. *Biochim. Biophys. Acta Bioenerg.* 1757:742–9.

Oliver, R. L., Whittington, J., Lorenz, Z. & Webster, I. T. 2003. The influence of vertical mixing on the photoinhibition of variable chlorophyll a fluorescence and its inclusion in a model of phytoplankton photosynthesis. *J. Plankton Res.* 25:1107–29.

Pearson, P. N. & Palmer, M. R. 2000. Atmospheric carbon dioxide concentrations over the past 60 million years. *Nature* 406: 695–9.

Peng, T. H., Takahashi, T., Broecker, W. S. & Olafsson, J. 1987. Seasonal variability of carbon dioxide, nutrients and oxygen in the North Atlantic surface water: observations and a model. *Tellus* 39B:439–58.

Quigg, A., Finkel, Z. V., Irwin, A. J., Rosenthal, Y., Ho, T. Y., Reinfelder, J. R., Schofield, O., Morel, F. M. M. & Falkowski, P. G. 2003. The evolutionary inheritance of elemental stoichiometry in marine phytoplankton. *Nature* 425:291–4.

Ragni, M., Airs, R. L., Leonardos, N. & Geider, R. J. 2008. Photoinhibition of PSII in *Emiliania huxleyi* (Haptophyta) under high light stress: the roles of photoacclimation, photoprotection, and photorepair. *J. Phycol.* 44:670–83.

Riebesell, U., Zondervan, I., Rost, B., Tortell, P. D., Zeebe, R. E. & Morel, F. M. M. 2000. Reduced calcification of marine plankton in response to increased atmospheric CO_2. *Nature* 407:364–7.

Rost, B. & Riebesell, U. 2004. Coccolithophores and the biological pump: responses to environmental changes. *In* Thierstein, H. R. & Young, J. R. [Eds.] *Coccolithophores: From Molecular Processes to Global Impact*. Springer-Verlag, Berlin, pp. 99–125.

Rost, B., Zondervan, I. & Wolf-Gladrow, D. 2008. Sensitivity of phytoplankton to future changes in ocean carbonate chemistry: current knowledge, contradictions and research directions. *Mar. Ecol. Prog. Ser.* 373:227–37.

Sang, M., Ma, F., Xie, J., Chen, X. B., Wang, K. B., Qin, X. C., Wang, W. D., Zhao, J. Q., Li, L. B., Zhang, J. P. & Kuang, T. Y. 2010. High-light induced singlet oxygen formation in cytochrome b_6f complex from *Bryopsis corticulans* as detected by EPR spectroscopy. *Biophys. Chem.* 146:7–12.

Satoh, D., Hiraoka, Y., Colman, B. & Matsuda, Y. 2001. Physiological and molecular biological characterization of intracellular carbonic anhydrase from the marine diatom *Phaeodactylum tricornutum*. *Plant Physiol.* 126:1459–70.

Sciandra, A., Harlay, J., Lefevre, D., Lemee, R., Rimmelin, P., Denis, M. & Gattuso, J. P. 2003. Response of coccolithophorid *Emiliania huxleyi* to elevated partial pressure of CO_2 under nitrogen limitation. *Mar. Ecol. Prog. Ser.* 261:111–22.

Shi, D., Xu, Y. & Morel, F. M. M. 2009. Effects of the pH/pCO_2 control method on medium chemistry and phytoplankton growth. *Biogeosciences* 6:1199–1207.

Six, C., Finkel, Z. V., Irwin, A. J. & Campbell, D. A. 2007. Light variability illuminates niche-partitioning among marine picocyanobacteria. *PLoS ONE* 2: e1341, DOI: 10.1371/journal.pone.0001341.

Smetacek, V. 1999. Diatoms and the ocean carbon cycle. *Protist* 150:25–32.

SPSS Inc. 2008. *SPSS for Windows Rel. 17.0.1.* SPSS Inc., Chicago, Illinois.

Suh, H. J., Kim, C. S. & Jung., J. 2000. Cytochrome b6/f complex as an indigenous photodynamic generator of singlet oxygen in thylakoid membranes. *Photochem. Photobiol.* 71:103–9.

Tcherkez, G. G. B., Farquhar, G. D. & Andrews, T. J. 2006. Despite slow catalysis and confused substrate specificity, all ribulose bisphosphate carboxylases may be nearly perfectly optimized. *Proc. Natl. Acad. Sci. U. S. A.* 103:7246–51.

Tortell, P. D., Ditullio, G. R., Sigman, D. M. & Morel, F. M. M. 2002. CO_2 effects on taxonomic composition and nutrient utilization in an Equatorial Pacific phytoplankton assemblage. *Mar. Ecol. Prog. Ser.* 236:37–43.

Tortell, P. D., Payne, C. D., Li, Y. Y., Trimborn, S., Rost, B., Smith, W. O., Riesselman, C., Dunbar, R. B., Sedwick, P. & Ditullio, G. R. 2008. CO_2 sensitivity of Southern Ocean phytoplankton. *Geophys. Res. Lett.* 35: L04605, DOI: 10.1029/2007GL032583.

Wu, H., Cockshutt, A. M., McCarthy, A. & Campbell, D. A. 2011. Distinctive PSII photoinactivation and protein dynamics in marine diatoms. *Plant Physiol.* 156:2184–95.

Wu, Y., Gao, K. & Riebesell, U. 2010. CO_2-induced seawater acidification affects physiological performance of the marine diatom *Phaeodactylum tricornutum. Biogeosci. Disc.* 7:3855–78.

Zapata, M., Rodriguez, F. & Garrido, J. L. 2000. Separation of chlorophylls and carotenoids from marine phytoplankton: a new HPLC method using a reversed phase C-8 column and pyridine-containing mobile phases. *Mar. Ecol. Prog. Ser.* 195: 29–45.

Zeebe, R. E. & Wolf-Gladrow, D. A. 2001. *CO_2 in Seawater: Equilibrium, Kinetics, Isotopes.* Elsevier Oceanography Series, 65. Elsevier Science, Amsterdam, the Netherlands, 346 pp.

Zondervan, I., Zeebe, R. E., Rost, B. & Riebesell, U. 2001. Decreasing marine biogenic calcification: a negative feedback on rising atmospheric pCO_2. *Glob. Biogeochem. Cycle* 15:507–16.